Space Launch System Base Heating Test: Environments and Base Flow Physics

Manish Mehta[1], Kyle S. Knox[2], C. Mark Seaford[3]
NASA Marshall Space Flight Center, Huntsville, Alabama, 35812

and

Aaron T. Dufrene[4]
CUBRC Inc., Buffalo, New York, 14225

The NASA Space Launch System (SLS) vehicle is composed of four RS-25 liquid oxygen-hydrogen rocket engines in the core-stage and two 5-segment solid rocket boosters and as a result six hot supersonic plumes interact within the aft section of the vehicle during flight. Due to the complex nature of rocket plume-induced flows within the launch vehicle base during ascent and a new vehicle configuration, sub-scale wind tunnel testing is required to reduce SLS base convective environment uncertainty and design risk levels. This hot-fire test program was conducted at the CUBRC Large Energy National Shock (LENS) II short-duration test facility to simulate flight from altitudes of 50 kft to 210 kft. The test program is a challenging and innovative effort that has not been attempted in 40+ years for a NASA vehicle. This paper discusses the various trends of base convective heat flux and pressure as a function of altitude at various locations within the core-stage and booster base regions of the two-percent SLS wind tunnel model. In-depth understanding of the base flow physics is presented using the test data, infrared high-speed imaging and theory. The normalized test design environments are compared to various NASA semi-empirical numerical models to determine exceedance and conservatism of the flight scaled test-derived base design environments. Brief discussion of thermal impact to the launch vehicle base components is also presented.

Nomenclature

$\mathrm{Re} = \dfrac{\rho U D}{\mu}$

$\mathrm{Pr} = \dfrac{\rho c_p}{k}$

$\dot{q}$ = heat flux $\left(\dfrac{BTU}{ft^2 - \sec}\right)$

$\dot{m}$ = mass flow rate $\left(\dfrac{lbm}{\sec}\right)$

ρ = gas densityy (lb/ft^3)

U = gas velocity (ft/sec)

μ = gas viscosity (psi-sec)

c_p = specific heat at constant pressure (BTU/lbm-deg R)

k = thermal conductivity (BTU/sec-deg R - in)

T = static temperature (deg R)

P = static pressure (psia)

D = nozzle exit diameter (inch)

Subscripts

$c, base$ = test-derived flight convective heating rates in the base

$arbitrary$ = heating rate at an arbitrary location on the vehicle

$b, base$ = base

$test$ = wind tunnel test

$flight$ = flight conditions

c = combustion chamber

∞, inf = freestream

lip = nozzle lip conditions

g = base gas

---

[1] Aerospace Engineer, Aerothermodynamics, Aerosciences Branch, MS 3421/EV33, AIAA Member,
[2] Aerospace Engineer, Aerothermodynamics, Qualis-Jacobs Inc., MS 3416/EV33, AIAA Member
[3] Aerospace Engineer, Aerothermodynamics, Aerosciences Branch, MS 3420/EV33, AIAA Member
[4] Senior Research Scientist, Aerothermal and Aero-Optics Evaluation Center, AIAA Member

I. Introduction

THE U.S. Space Launch System (SLS) shown in Figure 1 will provide an entirely new capability for human exploration beyond low-Earth orbit. The NASA George C. Marshall Space Flight Center is leading the design and development of SLS that will enable humans to go to the Moon, asteroids, LaGrange points, and eventually to Mars, continuing America's journey of discovery of space. The SLS is designed to be an evolvable system with expanding capabilities[1]. The initial Block 1 vehicle will have a lift capability of 70 Tons (t) and will eventually evolve to a Block 2 configuration with a lift capability of 130t. The SLS will be propelled with four liquid hydrogen (LH_2) and liquid oxygen (LO_2) rocket engines and two five-segment solid rocket boosters (SRB)[1].

The LH_2/ LO_2 RS-25 rocket engines were the highly robust and efficient space shuttle main engines (SSME). These engines will be repurposed for the SLS vehicle and arranged into a square within the base as shown in Figure 1. The main thrust for the initial ~100 seconds is provided by two five-segment polybutadiene acrylonitrile (PBAN) reusable solid rocket motors (RSRMV) which are mounted on either side of the core-stage[2]. The SLS Block 1 vehicle includes the Orion Multi-Purpose Crew Vehicle (MPCV), which consists of a Launch Abort System (LAS), Crew Module, Service Module and Spacecraft Adapter Jettison panels. Also included are a Launch Vehicle Stage Adapter (LVSA), an Interim Cryogenic Propulsion Stage (ICPS), an MPCV Stage Adapter (MSA) and an additional Spacecraft Adapter[1].

There are various base components for the vehicle that are instrumental for mission success. The base heat shield (BHS) protects the base of the vehicle and its' internal components from excessive heating. NASA is proposing to use cork for the BHS. The engine-mounted heat shield (EMHS) protects RS-25 turbopump machinery and gimbal actuators. A thermal blanket is being proposed for the EMHS and this is described in more detail in later sections. The SRB thermal curtain protects the motor gimbal actuators and electronics from high heating and will be similar to NASA STS Shuttle design. There are other important base components that could be sensitive to high heating rates and loads such as the boat-tail (BT), the booster separation motors (BSM), the SRB aft-skirt and the aft-skirt aft attach struts as shown in Figure 1. The RS-25 and RSRMV nozzles could also be sensitive to plume induced heating. These loads may have an effect on the RSRMV liner to housing adhesive bondline. The excessive heating areas of concern for the RS-25 nozzles are the hat-bands, drain lines, fuel transfer ducts and support brackets. These components need to be within the appropriate substrate temperature range during the vehicle flight to prevent catastrophic failure. As a result, heating rates and heat load need to be accurately predicted to appropriately design the thermal protection system (TPS) for these components.

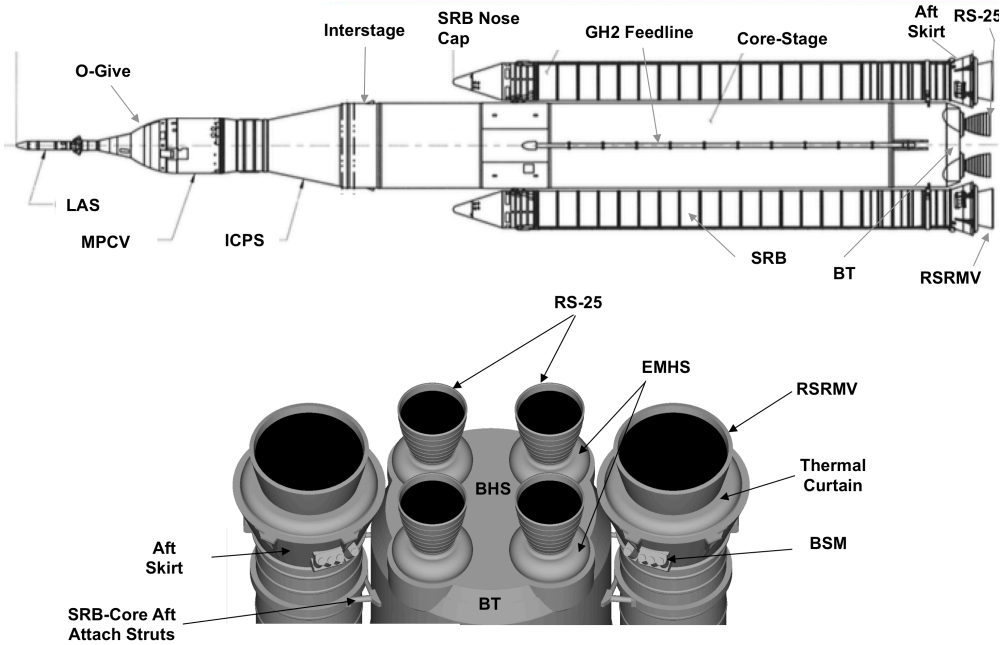

Fig 1. Schematic of SLS-10005 (top) and base components (bottom)

NASA collaborated with CUBRC for four years to develop a SLS base heating test program, referred also as ATA-002 within the SLS Program. Prior to conducting a high fidelity sub-scale convective base heating test program, robust and similarly performing SLS model propulsion systems were necessary for a successful test program. A two-percent RS-25 gaseous oxygen and hydrogen rocket engine with similar performance to the flight engine was designed and developed for ATA-002 as described by *Mehta et al* [2014][3]. The model booster propulsion system was also successfully developed for the base heating test with similar performance to the full-scale RSRMV as described by *Mehta et al* [2014][4]. Once the SLS model propulsion systems were successfully developed and tested during the Pathfinder test program, the SLS forebody was designed and fabricated as shown in Figure 2. The core-stage and full-stack ATA-002 model configurations are shown in Figure 2 within the CUBRC LENS II facility. The core-only configuration does not have the SRBs side-mounted to the core-stage. *Dufrene et al* [2016] describes in-detail the test operation, non-intrusive diagnostics, instrumentation type and layout, model description, propulsion system and facility performances, test matrix and objectives, data reduction methods and raw test data results for the SLS base heating test program, which was successfully completed in September 2016[4]. This paper investigates the base flow physics and presents normalized test-derived external thermal design environments for the SLS base region from lift-off to main-engine-cut-off (MECO). The base flow physics and environments for this vehicle are considerably different from previous heritage launch vehicles.

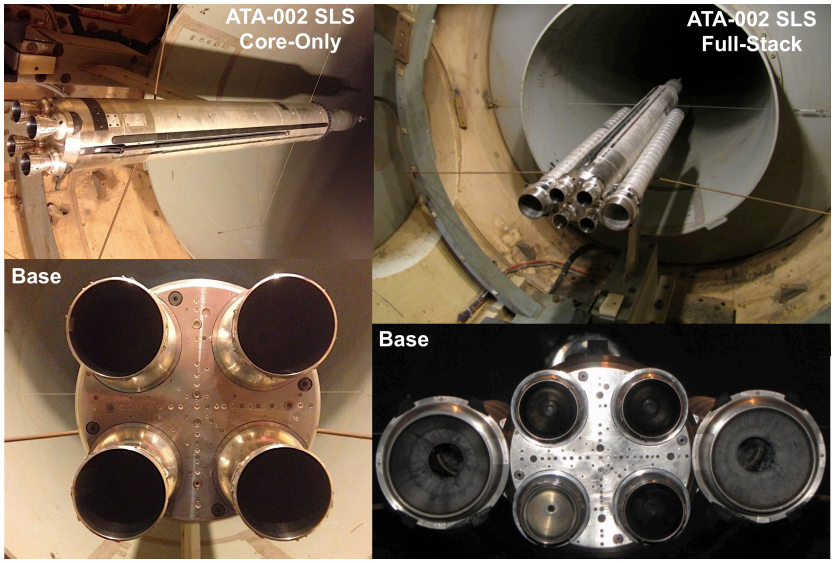

Fig 2. Two-percent SLS-100005 ATA-002 wind tunnel model

II. Base Flow Physics

A. General Base Flow Theory

Launch vehicle base flow physics have been investigated and flow processes observed during past sub-scale wind tunnel and flight tests in support of previous vehicles such as the NASA Space Shuttle and Saturn Programs[5]. Semi-empirical engineering tools have been developed to incorporate test data of previous flight vehicles for predicting base flow behavior of new vehicles. Computational fluid dynamics (CFD) models have been used to further investigate base flows for single and multi-rocket engine vehicle configurations and have been compared to test data. Multi-rocket plume induced base flow is highly complex due to various flow structures, flow regimes and large thermal and momentum gradients within the base region as shown in Figure 3. Such flows span from subsonic to supersonic fluid dynamics regimes and from extremely cold boundary layer flows over propellant feedlines to extremely hot rocket plume internal nozzle flows. These extreme environments make base flows challenging but also critical to assess

and predict to prevent vehicle failure. Hence, NASA Marshall's Aerosciences Branch has spent the last fifty years in investigating and predicting base flows for launch vehicles.

To accurately predict and understand the base flow physics, boundary and input conditions and internal flow of various types of propulsion systems such as liquid, solid and hybrid systems need to be accurately defined. Flight path trajectories and freestream conditions need to be determined. Base configuration such as number of engines and rocket motors and their layout within the aft section of the launch vehicle should be known prior to assessment. This requires the merging of many technical disciplines such as propulsion, guidance, navigation and controls (GN&C), thermal and aerothermodynamics. Figure 3 shows a schematic of the various base flow regimes during launch vehicle ascent from lift-off to in-space environments. Figure 4 shows the classic 4-engine vehicle model where base flow theory for multiple-engines is developed[6]. These three regimes have been observed for all flight NASA launch vehicles. The onset and duration of these regimes varies depending on the parameters described above such as flight trajectories, propulsion parametrics, base configuration, etc.

When the rocket with multiple engines is on the launch pad at NASA Kennedy Space Center and all engines have ignited and are burning, the rocket plume exhaust at the nozzle exit is at high supersonic speeds with a large mass flow rate. The four engine supersonic rocket plumes at the nozzle exit entrain the surrounding cold freestream air into the base region. Figure 3 only shows the cross section through the centerline of two engines. These rocket engines act as efficient ejectors at low altitudes. The rocket plumes are highly over-expanded and form well defined Mach discs. Due to a lower nozzle exit pressure than the freestream, this causes the streamlines to converge toward the center of the flow and form a characteristic Mach disc to rapidly equilibrate the plume pressure with the ambient. This shock structure for over-expanded jets prevents the nozzle boundary layer flow and jet shock from interacting with adjacent surrounding rocket plumes. There is no plume-plume interaction in this regime. This leads to large cold freestream entrainment and the air entrains into all vent regions within the base and merges near the base center to form an entrained stream as shown in Figure 3. This leads to significant cooling and evacuation of pressure at the base, which causes negative convective heat fluxes and base pressure differentials. As the vehicle ascends off the launch pad and gains velocity, it begins to entrain more freestream air into the base that leads to more convective cooling and lower base pressure differential. The peak aspiration point occurs at an altitude when the entrained air stream has the largest momentum component. This is described as the aspiration flow regime.

As the vehicle ascends to higher altitudes, the freestream pressure decreases with altitude, but the nozzle exit pressure is fixed for a constant thrust profile. This causes the plume shock structure to change from over-expanded to moderately under-expanded which leads to expansion of the plumes and the Mach disc to change from a Mach disc reflection to a regular reflection. Due to an increase in plume expansion, the jet shocks begin to minimally interact with adjacent plumes, leading to a stagnation point at the intersection point of the two jet shocks downstream from the nozzle exit plane. An adverse pressure gradient begins to form downstream of the stagnation point. This pressure gradient in the wake of the plume-plume interaction region causes lower energy nozzle boundary layer flow to be diverted upstream towards the BHS. Most of the rocket plume mass flux flows axially away from the base and is termed the inviscid core region. Within the transition regime, an updraft plume begins, but it competes with the entrained stream. The axial momentum component is equivalent between the updraft plume and entrained stream at the transition point. At the transition point, the updraft plume and entrained stream momentum vector components cancel each other which null the convective heating and pressure differential at the base. The transition point of base flows is a critical parameter to accurately determine for TPS design, because it defines the total base heat load for a vehicle.

As the vehicle ascends to very high altitudes, the freestream pressure further decreases and approaches near vacuum while the thrust profile is fixed. This leads to highly under-expanded plumes and significant plume expansion as shown in Figure 3. High plume-plume interactions are observed with a stagnation point much closer to the nozzle exit plane and a much larger pressure gradient. This results in larger fraction of the nozzle boundary layer to flow upstream toward the base due to a higher pressure gradient. There is a smaller momentum component of the entrained stream due to a decrease in the atmospheric density and larger component of the updraft plume prevents freestream entrainment into the base. This results in recirculation flow near the periphery of the base and plume-induced flow separation (PIFS)[5]. As the altitude increases with fixed thrust profile, the pressure gradient increases and the updraft plume velocity increases and approaches supersonic speeds. At supersonic updraft plume velocities, a normal recovery shock develops upstream of the base which results in high stagnation convective heating. Once the flow

stagnates at the base, a wall jet propagates outward from the stagnation point, which further prevents freestream entrainment into the base. Recirculation flow of the shear layer develops between the updraft plume and entrained air. These complex flow processes occur within the recirculation regime. There is a peak recirculation heating point where the updraft plume and freestream air are optimized within the base. Peak convective heating and base pressure occur at this altitude point. Peak base pressure and heating do not necessarily occur at the same altitude, but are similar. The mixing of the entrained air with oxygen and the hot updraft plume may result in ignition, which leads to afterburning within the base region. This can significantly increase convective heating, which could lead to base burning and vehicle failure if not considered in vehicle design.

When the updraft plume mass flow rate is constant through the vent regions in the base, the base flow enters choked recirculation flow regime. During this regime, the updraft plume and wall jet achieve supersonic velocities. This prevents freestream air entrainment and constant heating rates and base pressures are observed. The constant pressure and heating rates of recirculation choked flow is entirely dependent on the thrust profile of the rocket engines and the heating decreases as the engine chamber pressure decreases. The flow physics described here are for multiple rocket engines with a fixed thrust profile that are attached to the base and protected by a flat BHS as shown in Figure 4. The flow physics and base thermal environments for the four-engine configuration have been studied extensively in the past[3]. However, the base flow physics for SLS are considerably different.

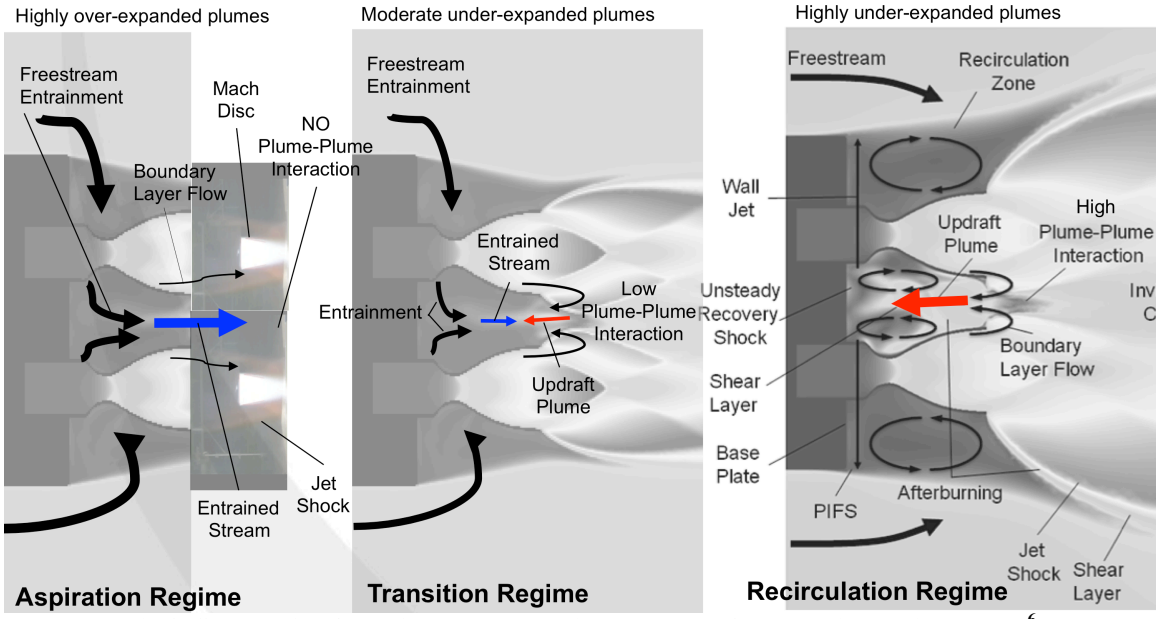

Fig 3. Schematic of multi-rocket plume induced base flow physics during ascent[6]

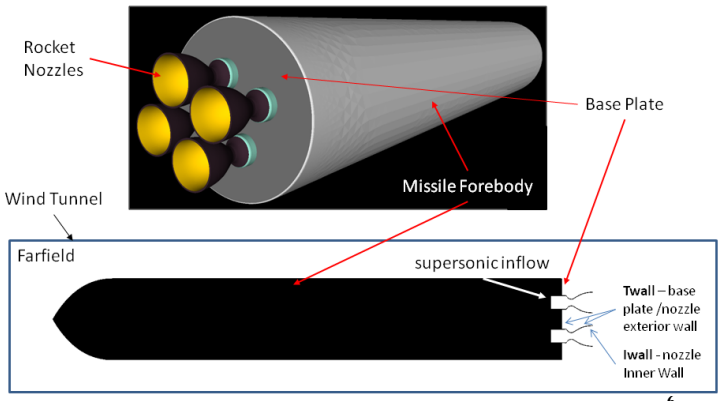

Fig 4. Schematic of generic multi-rocket engine vehicle[6]

B. SLS Base Flow Physics

There are a number of factors that separate the base flow physics for SLS compared to previous launch vehicles. The first and most important aspect is the unknown influence of the close proximity of the SRBs to the BHS. This was not the case for the NASA Shuttle program where the SRBs are far removed from the Orbiter base. The unknown interaction effects of the RSRMV plumes with the RS-25 plumes may alter the generic base flow model. The second factor is the non-fixed thrust profile of the SLS vehicle during the entire flight trajectory. The RSRMV thrust profile is not fixed and changes as a function of altitude. For example in one instant, the RSRMV thrust tails-off prior to SRB separation. The third factor is that solid aluminum-oxide particle entrainment due to the RSRMV plumes has an unknown effect on the base flow. The solid particles affect the RSRM plume expansion and alter the momentum and energy transfer of the plumes, and these hot particles may convect towards the base. The fourth factor is the normalized nozzle spacing, the ratio distance between the centerline of two nozzles and nozzle exit diameter, is considerably different between SLS and heritage launch vehicles. This may affect the flow and convective and radiation heating components. Other factors such as the geometry of the EMHS, RS-25 nozzles and the SRB base may locally influence base flow. As a result, there are many factors that may result in differences in the base flow of SLS as compared to previous heritage launch vehicles.

Figure 5 shows the proposed base flow process for the SLS full-stack vehicle during the recirculation regime. This SLS base flow model proposed is based on test data, theory and IR imaging. During the transition and recirculation regimes, the RS-25 plume incident shocks from the nozzle exit interact and form reflected shocks. The incident shocks or jet shocks cause the nozzle flow pathlines to propagate towards each other as shown by B and Q pathlines. Incident shocks are formed due to Prandtl-Meyer expansion and reflected shocks are formed because the nozzle flow streamlines cannot cross paths due to the velocity vector having a unique solution. This results in the RS-25 core plumes to flow in parallel as shown in C and R path lines shown in Figure 5. This is known as the Edney shock-shock type 1 interaction. The Edney shock-shock type 1 interaction yields a large stagnation pressure point and the reflected shocks are the boundaries for the reflected shock fan[7]. These inviscid flow structures are important in the development of base flows.

High kinetic energy nozzle boundary layer constitutes most of the flow within reflected shock fan. This flow can pass across the large pressure gradient formed by the reflected shocks. As can be seen in Figure 5, the reflected shock fan directs the base flow (low kinetic energy nozzle boundary layer) either towards the center of the BHS or outward towards the periphery through the vent regions[6]. The reflected shock fans are formed between adjacent RS-25 plumes through the Edney shock-shock type 1 interactions. There are four reflected shock fans that direct the updraft plume (base flow) towards the BHS center as shown by the red arrows. Once the updraft plume impinges on the base center, which is shown as the base stagnation region, four wall jets form at 45 degrees clocking angles from the incoming base flow. The wall jet is constrained from the incoming base flows and strong adverse pressure gradient due to the reflected shock fans. This results in the impingement of the wall jet on the in-board region of the EMHS and shown as the EMHS stagnation region in Figure 5. The CFD streamlines support the proposed SLS base flow model (Figure 5). This describes the SLS core base flow physics due to the RS-25 plumes. The booster plumes interact with the RS-25 plumes and develop a base periphery stagnation region. Booster plume flow physics will be discussed in later sections.

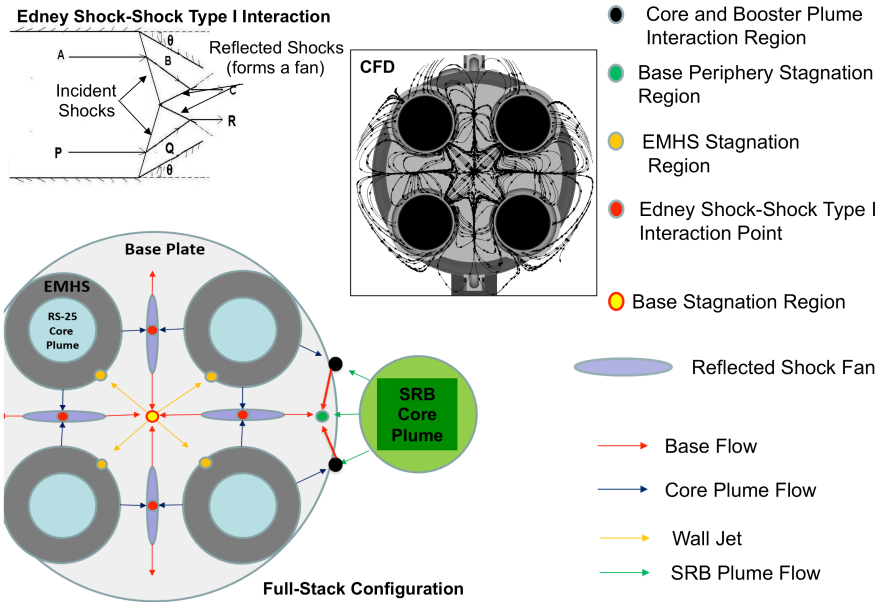

Fig 5. Schematic of SLS base flow physics during recirculation regime

C. Flow Physics Supported by Surface Measurements

Figures 6 and 7 show the normalized convective base heat flux contours at different simulated altitudes from the ATA-002 test data. The thin-film heat transfer gauge layout is shown in the figure and the mean scaled to flight heat flux values are depicted on these contours. Linear interpolation and mirroring has been implemented with the test data to obtain a contour map of the BHS and EMHS. The ATA-002 test data has been scaled to flight and then normalized by an arbitrary surface vehicle heating location to show relative scale. As supporting the generic base flow model, the aspiration flow regime is dominated at low altitudes on the order of ~70 kft and below. It can be seen at 70 kft that the convective heat flux values are all uniform and low due to cold freestream entrainment flowing over the BHS and EMHS and a minor component of the updraft plume. As a result, there is virtually no wall jet impinging on the EMHS due to uniform and low heating rates similar to the BHS. The aspiration regime is denoted as I.

As the ATA-002 wind tunnel model is tested at higher simulated altitudes such as 106 kft, the convective heat flux contour changes. There is higher heating biased in the north-south (N-S) directions towards the vent areas of the BHS, and peak heating is observed within the base center. The in-board EMHS shows slightly higher heating rates than at 70 kft suggesting a larger wall jet momentum flux. This is denoted as the recirculation regime, IIa. It is hypothesized that the high heating biased towards the vent areas is due to the fact that RSRMV plumes are at full-throttle at this altitude and minimal RS-25 and RSRMV plume interactions are entraining periphery base flow from the reflected shock fans. This leads to an evacuation of the periphery near the SRBs and a drop in base pressure which in turn decreases the convective heat flux in this region between the two RS-25 engines and RSRMV. However, large entrainment is not observed at the vent areas, regions that are directly exposed to the freestream. This is due to low momentum freestream interacting with periphery directed base flows and resulting in a recirculation of plume-air at the vent areas. This leads to larger biased heating within the vent areas of the BHS.

At 121 kft, peak recirculation regime (denoted as II) is observed due to the characteristic high convective heating observed at the base center. This follows the conventional base flow model as described in Section 2a. A new flow regime, not observed from historical testing, is captured at 131 kft when the RSRMVs throttle-down prior to SRB separation. The SRB thrust is about 20% of the maximum thrust level. This directly influences the heating rate spatial distribution on the BHS. It can be observed from Figure 6 that higher heating is biased east-west (E-W) towards the SRBs. It is hypothesized that the reduced thrust at this altitude leads to a reduced RSRMV plume momentum and high plume-plume interactions with the RS-25 plumes. This results in localized base flow recirculation at the E-W BHS periphery as depicted in the schematic of Figure 5. This local recirculation results in an increase in the convective heat flux and base pressure as had shown in Figures 9 an 10. It should also be noted that the

base center heating rates are lower than E-W periphery region. This regime is denoted as the SRB tail-off effect, III.

After SRB separation and the four RS-25 engines are burning at a fixed thrust, the base flow behaves like the conventional four-engine base flow model as discussed in Section 2a. Peak heating is observed within the center and lower heating is seen at the periphery, which is due to large base flow component being directed to the center from the four reflected shock fans. The characteristic wall jets impinge on the in-board region of the EMHS, leading to high convective heating as shown in Figure 7. The base flow pattern is relatively similar between 156 kft and 211 kft. These flow processes occur in the choked recirculation regime, IV. It should be noted that half of the ATA-002 tests were conducted in the core-only flight configuration because maximum heat load on the base would be observed in this configuration with a core-only flight duration of ~400 seconds. It should also be noted that the peak center and in-board EMHS heating rates are similar at 1.1 times the arbitrary heating rates in the choked flow regime.

Normalized base pressure as a function of altitude is shown in Figure 8. The scaled to flight base pressure differential is normalized by an arbitrary static pressure. The transition point is defined as the altitude at which point the base pressure differential is zero. It can be seen that the localized transition point is different between the base center and SRB in-board base. The base center transition point is at ~65 kft and the SRB and mid-way base regions are at ~55kft. Transition point is dependent on engine layout within the base, thrust profile and the local flow physics.

Figure 9 shows normalized flight base pressure differential spatial profile along the BHS y- and z-centerlines at different simulated altitudes. Figure 10 shows normalized flight convective heating rate spatial profiles along the BHS y- and z- centerlines at different altitudes. Both of these figures are the mean spatial profiles with temporal variability uncertainty bands. Figure 10 shows that the peak recirculation regime, III, has the maximum convective heating rates at the base center and show a characteristic bell-shaped curve profile along the y and z-axes. The base center convective heat flux is ~1.8 times the arbitrary heating rates on the vehicle. This trend is consistent with general base flow models. As observed from the heating rate contour maps in Figure 6, the RSRMV plumes alter the conventional base flow models at altitudes of 106 kft and 131 kft. This is observed in Figure 9 and 10, which shows asymmetry in the base pressure and heat flux between the y and z centerline axes, unconventional from previous base flow models. As a result, simply adding the heating and pressure environments of an isolated core-only configuration and booster-only configuration is not adequate due to this complex flow physics. It should be noted for the core-only configuration at high altitudes the base pressure and heating rate spatial distribution is a characteristic bell-shaped curve with a maximum at the center. This distribution was observed for all tests above a simulated altitude of 150 kft.

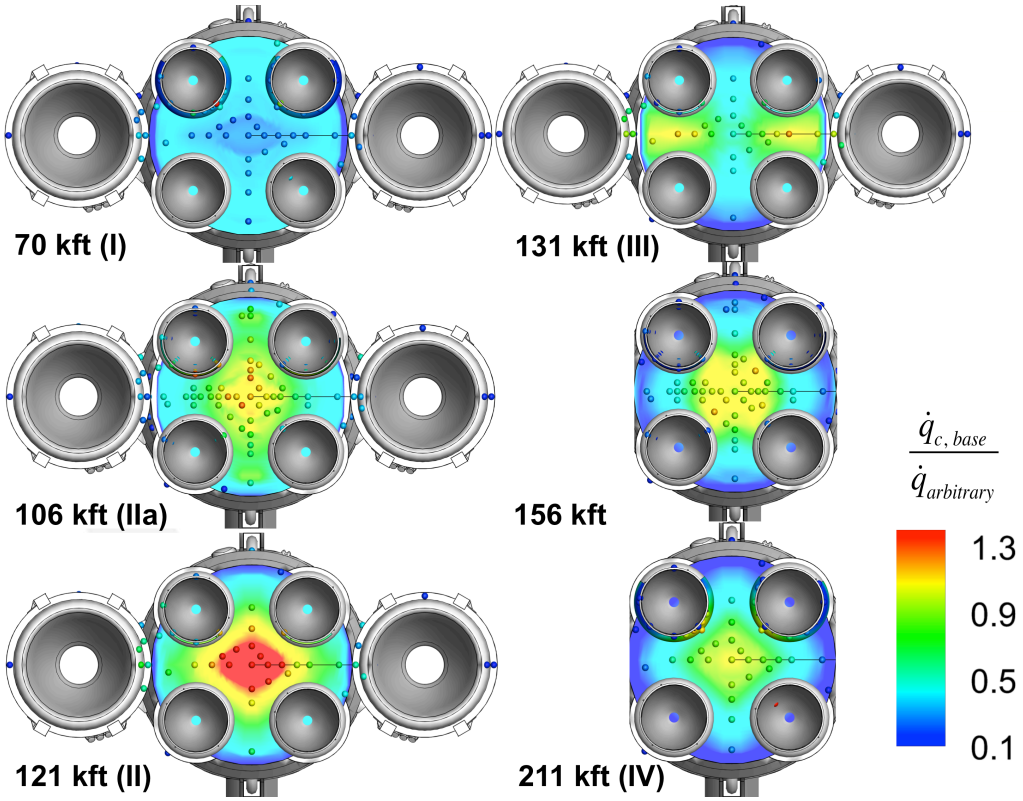

Fig 6. Normalized flight model-scaled convective heat flux contours of the BHS

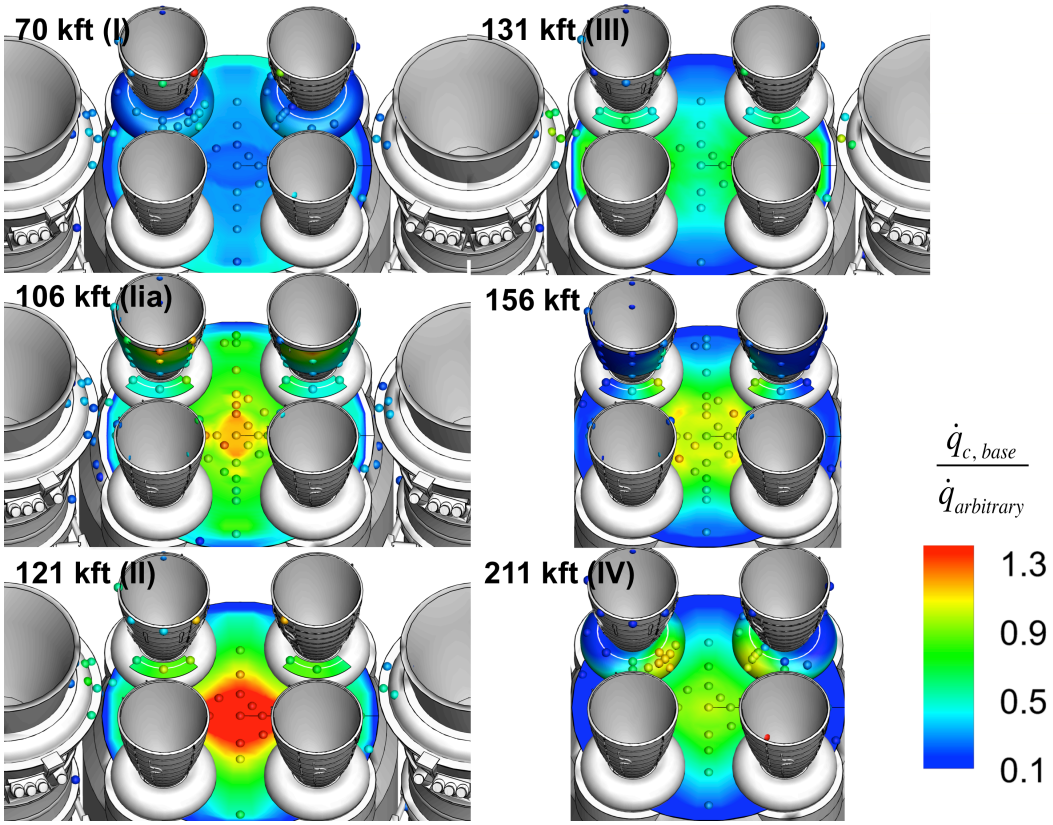

Fig 7. Normalized flight model-scaled convective heat flux contours of the EMHS

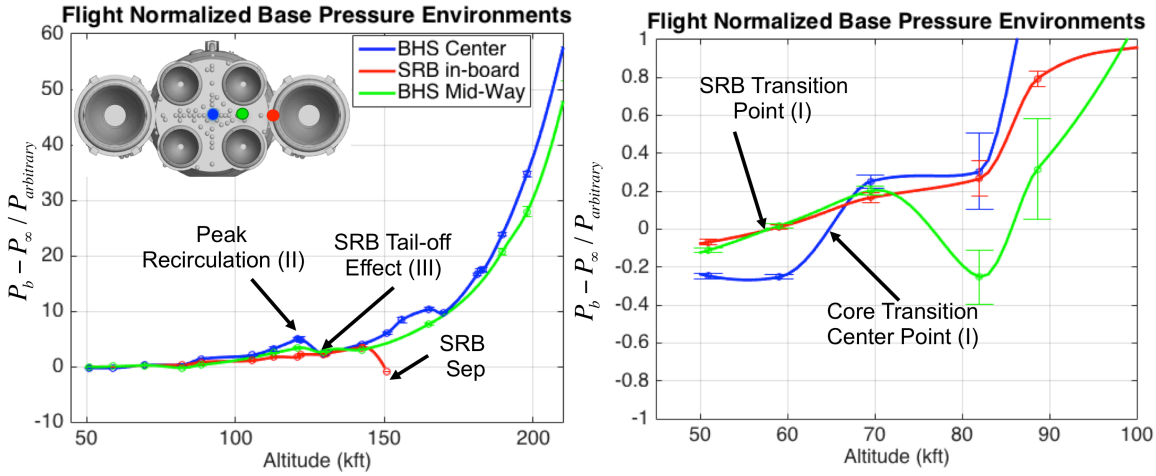

Fig 8. Normalized flight model-scaled base pressure as a function of altitude

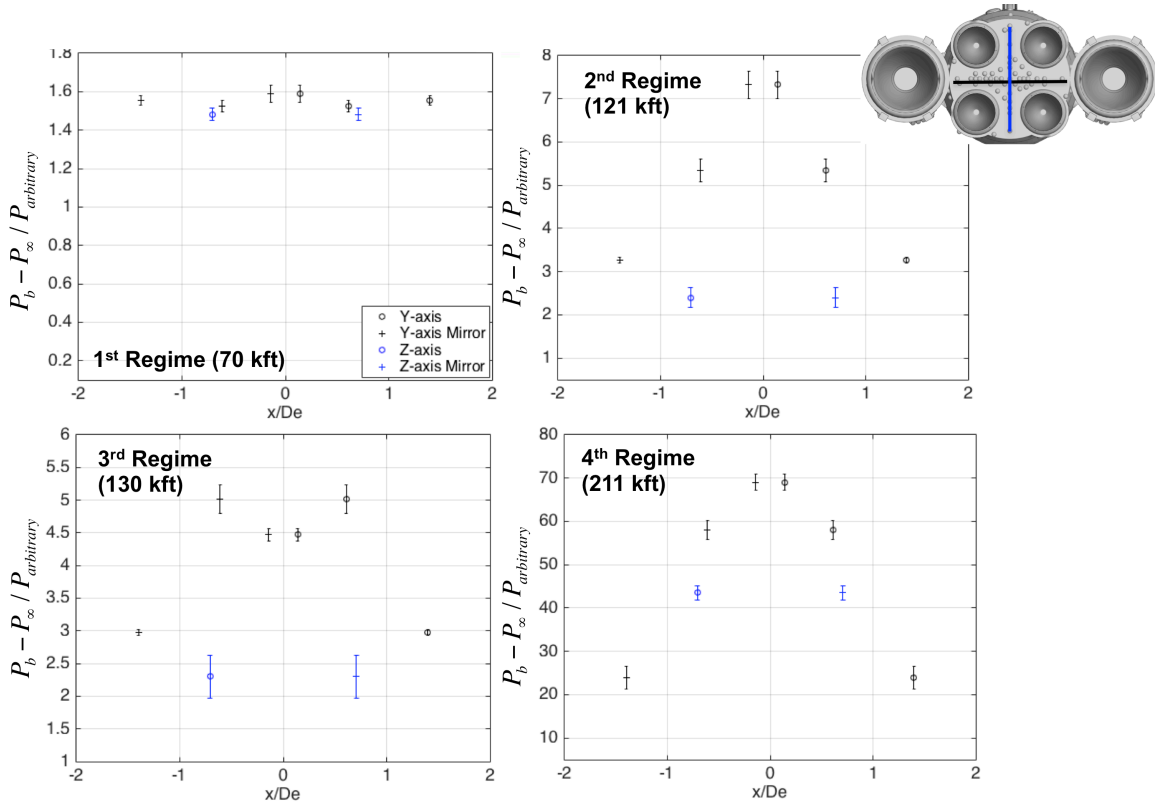

Fig 9. Normalized flight model-scaled base pressure spatial profile

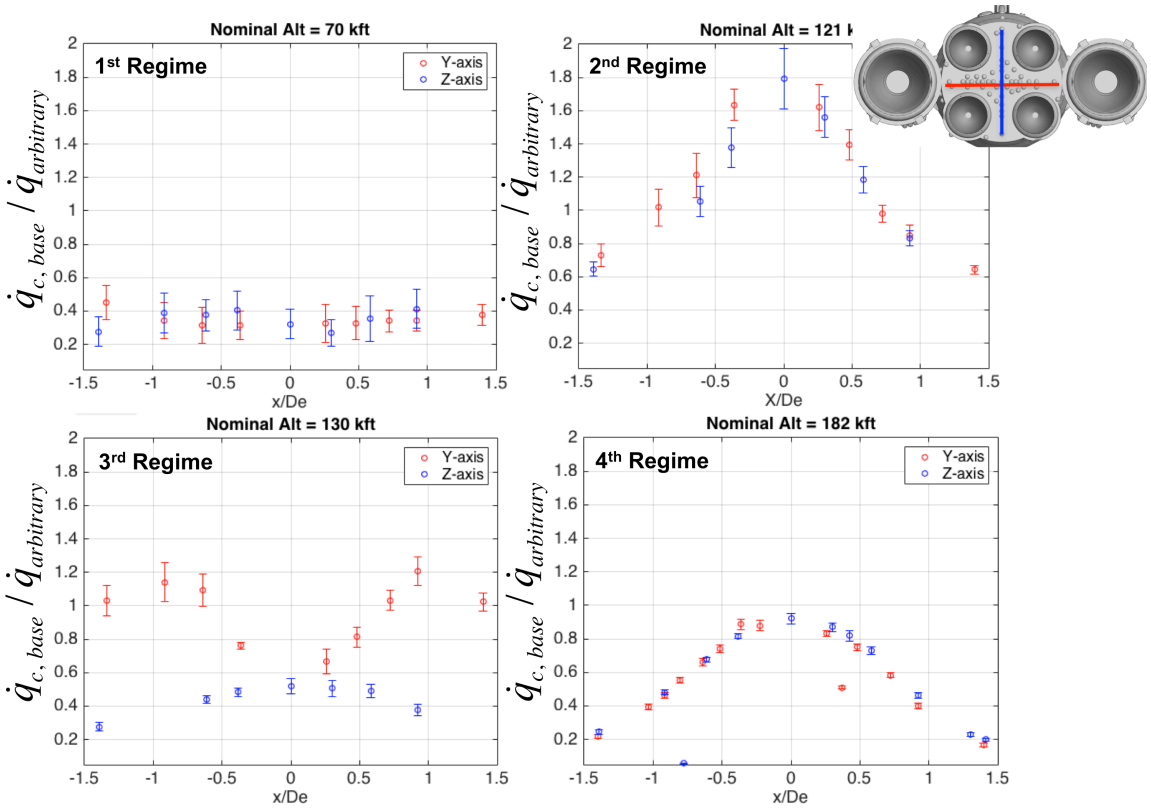

Fig 10. Normalized flight model-scaled base convective heat flux spatial profile

D. Flow Physics Supported by IR Imaging

Figure 11 which are long-wave infrared (LWIR) temperature contour maps provides more insight into the SLS base flow physics and the established SLS base flow model. These contour maps were taken at two different temperature sensitivities[11]: (a) low temperature sensitivity between 50 and 250 deg F and (b) high temperature sensitivity between 250 deg F and 1000 deg F. Two IR imagers were taken at the same focal length to increase the temperature dynamic range[11]. Blue contours refer to cool temperatures and red-white contours are peak temperature values. These are 20 millisecond (msec) time-averaged temperature maps during the steady-state data window. The RSRMV and RS-25 plumes and the base region are shown in the IR temperature maps. It can be seen that the RSRMV core plumes are much hotter than the RS-25D core plumes and this is partially due to hot aluminum-oxide particles and much smaller nozzle expansion ratio. The RSRMV plume expansion decreases between the three images due to a drop in motor throttle.

Most important feature of the IR temperature maps are the reflected shock fans, which are shown between the two RS-25 plumes. As the RS-25 plume expansion increases as a function of altitude, the Edney shock-shock type 1 stagnation point, the hottest point, and reflected shocks propagate closer to the RS-25 nozzle exit planes. The temperature of the reflected shock fan is strongly dependent on the temperature of the RSRMV plumes. In the recirculation regime, these booster plumes interact downstream of the core-engine RS-25 plumes, recirculate towards the center and interact with the reflected shock fans, increasing its' static temperature. The RSRMV plume temperatures directly influence the reflected shock fan and base flow temperature, which affects base heating. For example, the SRB tail-off effect at 131 kft shows a reduction on the static temperature for both the RSRM plumes and reflected shock fan. The static temperatures of both flow structures are high at full-throttle of the motor. It can be observed that the Edney shock-shock type 1 stagnation region and reflected shocks results in large temperature and pressure jumps as observed from the IR images. The RS-25 core plumes can be observed, but the full plume expansion cannot be seen due to low flow density. The LWIR images provide high fidelity detail to the plumes and strong inviscid flow structures, but are not able to capture base flow.

Figure 12 shows mid-wave infrared (MWIR) temperature contour maps of the base region at an altitude of 121 kft and 182 kft. The MWIR images were targeted to capture water absorption bands and two flow structures were clearly observed: (a) RS-25 plume expansion and (b) base flow stagnation. Although base flow streamlines cannot be observed, hot chaotic base flow structures are observed at 121 kft and a normal recovery shock of the updraft plume was formed at the base at 182 kft as shown in Figure 12. As a result, the high base gas density just upstream of the base is captured by the imager. It can be seen that the recovery shock impinges on the in-board EMHS. The plume expansion of the RS-25 plumes significantly increases between 121 kft and 182 kft. IR imaging shows the effects of the SRB plumes on the SLS base flow physics.

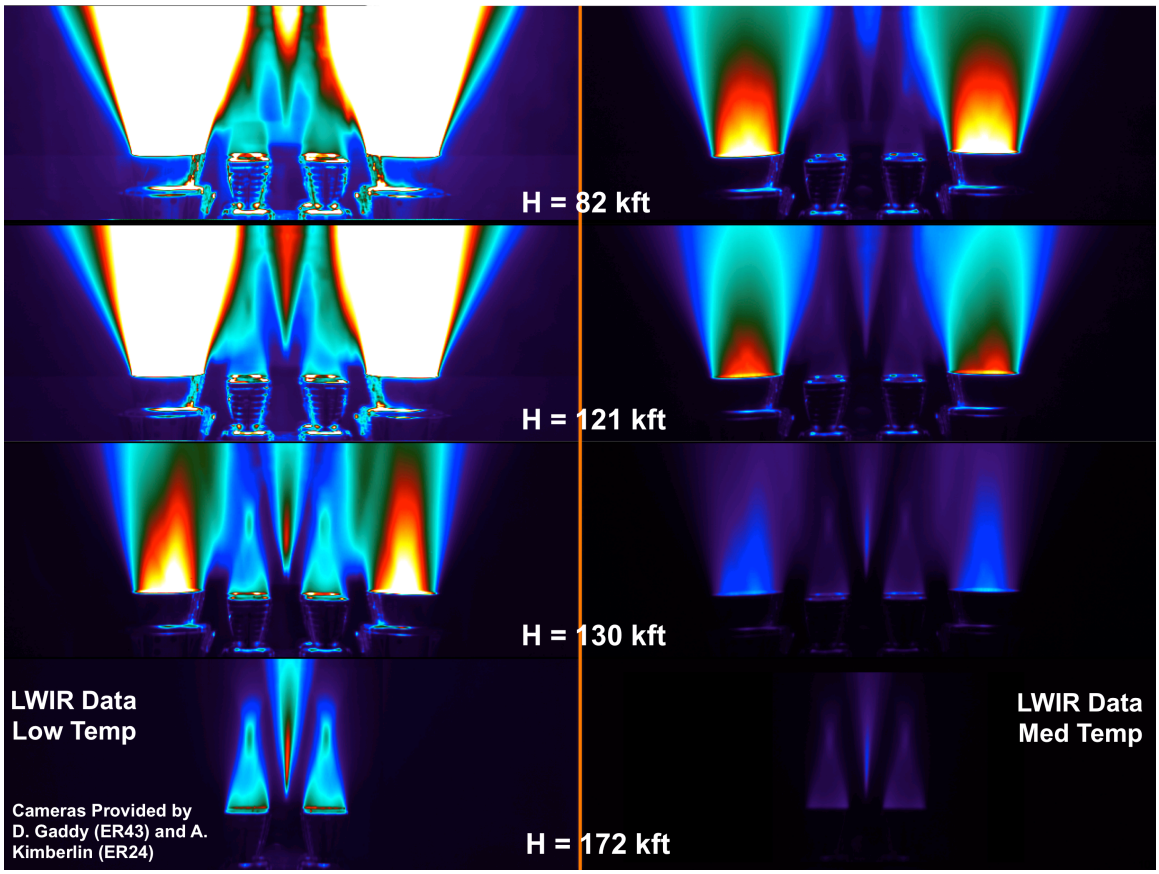

Fig 11. LWIR images of the ATA-002 SLS model base region at different altitudes

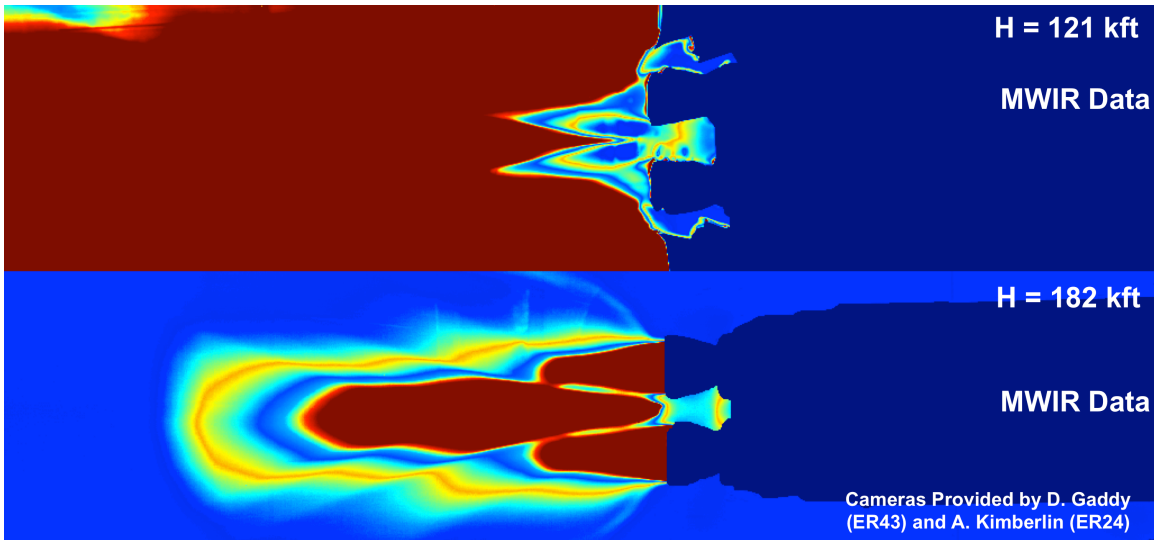

Fig 12. MWIR images of the ATA-002 SLS model base region at 121 kft (top) and 182 kft (bottom)

E. Test Data - Prediction Comparisons and Uncertainty Analysis

Figures 13-16 on the left-hand side show normalized test-derived flight convective heating rates as a function of altitude for the mean and mean + 1 sigma distributions to show the contribution of the uncertainty bands. Sigma is defined as one standard deviation of the temporal and spatial variability of the heating rates during the steady-state data window. These are the largest contribution to the uncertainty in the test data due to forcing a steady-state value in an unsteady flow environment. The temporal and spatial variability are obtained from mirror gauge surface measurements and repeat test runs. The total uncertainty is calculated by the root-sum square of these two variability components. The gauge uncertainty is a much smaller component. The steady-state data window as described in *Dufrene et al* [2016] occurs when the O/F ratio, chamber pressures and test section freestream pressure are quasi-steady and achieve target values[4]. These figures show nominal, one engine-out (1 EO), 2-degree RS-25 gimbal angle and 4-degree angle of attack (AoA) test cases. These figures target four base components: (1) BHS center, (2) 45-degree in-board EMHS region, (3) in-board SRB base region and (4) in-board RS-25 nozzle lip. The line profiles shown in red and black are linear interpolation of the normalized scaled nominal test data. The line profiles are averaged mirror gauges at the in-board EMHS (Figure 14), in-board SRB base (Figure 15) and in-board RS-25 nozzle lip (Figure 16). Larger uncertainty bands are observed at lower altitudes than high altitudes for all base components except the EMHS. Larger base flow unsteadiness occurs from the boosters firing and a larger freestream momentum component. The EMHS temporal variability component is small for core-only flight, but the spatial variability is large. This is due to a high wall jet clocking angle variability which depends on the clocking variability of the reflected shock fans and in-turn stems from RS-25 thrust differences between the four engines.

Figures 13-16 on the right-hand side show a comparison of normalized test-derived flight convective heating rates as a function of altitude between prediction and test data for nominal flight. The mean prediction profiles were developed from NASA semi-empirical model results prior to the ATA-002 test program[12]. The test data curve fit is a linear interpolation of the normalized scaled-to-flight nominal test data. The onset of these base flow regimes, described in earlier sections, are marked on these figures to further support findings of the SLS base flow physics. The onset of two events, not described in earlier sections, are the powered explicit-guidance maneuver (PEG) and SRB separation (SRB Sep). The PEG will be described in more detail in Section 3.

There were many findings from these figures that led to the SLS base flow physics model. It can be seen in the core-stage base area such as the BHS and EMHS, the normalized heating rates increase as function of altitude from the transition point to peak recirculation at 121 kft. There is a sudden drop off at 131 kft due to the SRB tail-off effect as observed from the contour plots. There is a jump in the normalized heating rates when the booster thrust tails-off to less than 10% just prior to SRB separation at ~145 kft. There is a hump in the heating rates due to the PEG maneuver (described in a later section), which occurs between

155 kft and 165 kft. After ~170 kft, choked base flow is observed with relatively constant heating rate as function of altitude as shown in Figures 13 and 14. The BHS center peak convective heating rate is ~2 times the arbitrary heating rate which is about 1.5 times higher than prediction. During the choked base flow regime, the normalized heating rates from test data are ~4 times that of the prediction results.

The current NASA semi-empirical models do not adequately capture the RSRMV plume effects on the base, high heating during core-only flight and the onset of transition. The transition point and peak recirculation occur at much higher altitudes than prediction. There is an off-set of ~45 kft and this is predominantly due to engine configuration within the base. The semi-empirical models were developed using Shuttle-derived data or similar to Shuttle which has a RS-25 normalized nozzle spacing of 1.2. The SLS vehicle has a normalized nozzle spacing of 2.5. Normalized nozzle spacing is conventionally chosen as the distance between diagonal engine centerlines over the nozzle exit diameter. This increased SLS nozzle spacing as compared to Shuttle leads to a delayed plume-plume interaction which delays the onset of transition and peak recirculation. Larger plume expansion angle is needed for plume-plume interactions to occur than prediction. It is also hypothesized from the test data that a larger volume within the SLS base due to an increase in nozzle spacing can allow a higher flow rate of the updraft plume to stagnate and recirculate, leading to higher base heating than prediction as observed in Figures 13 and 14. This also supports the finding of very low heating for the RS-25 in-board nozzle lip as shown in Figure 16. It shows that the nozzle spacing is large enough that the updraft plume does not interact or impinge on the nozzle lip as observed during the Shuttle base heating tests.

The SRB tail-off effect shows a decrease in the heating rates for the EMHS and BHS, but peak heating at the SRB in-board base region as shown in Figures 13-15. This is due to the hot zone moving from the base center to the E-W periphery and SRB in-board base regions during the SRB tail-off event. The RSRMV plume momentum with respect to the RS-25 plumes directly influences this effect. During the peak recirculation regime, the RSRMV plume momentum is much higher than the RS-25 plumes and the booster plumes interact with each other further downstream and contribute in energy and mass flow to the core base flow. The RSRMV plumes are not hindered by the expanding RS-25 plumes. This results in peak base pressure and heating at the BHS center as shown in Figure 13. During the SRB tail-off event, the booster plume momentum is less than or comparable to the RS-25 plumes which leads to RSRMV-RS-25 plume-plume interactions and local recirculation in the E-W periphery. As a result, the influence of the booster plumes to the core base flow is significantly diminished and peak heating is observed at the E-W and SRB in-board regions. The current semi-empirical models do not capture the heating effects due to RSRMV throttling and increased core-engine nozzle spacing.

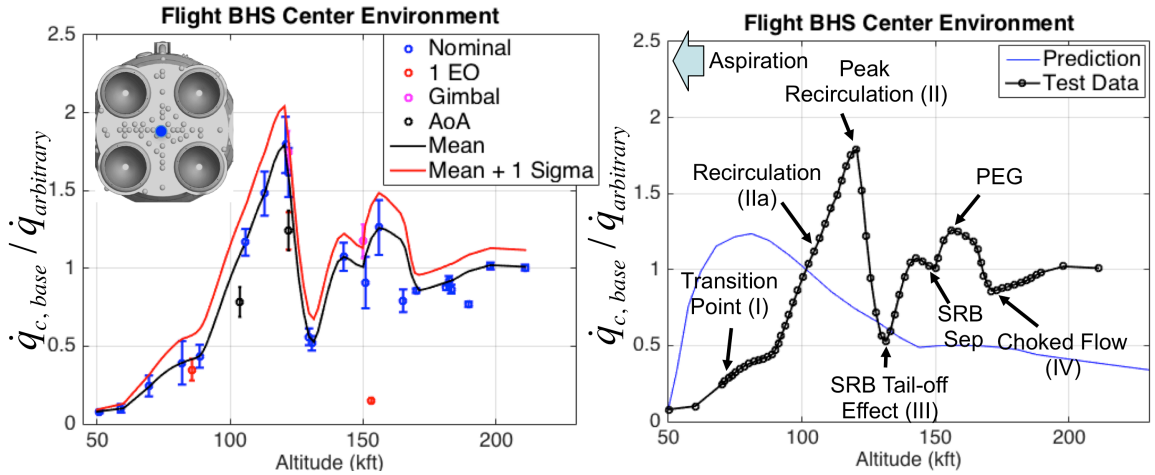

Fig 13. Normalized flight mean and mean + 1 sigma convective heat flux test data vs. altitude (left) and normalized flight mean test data and prediction heat flux vs. altitude at the BHS center (right)

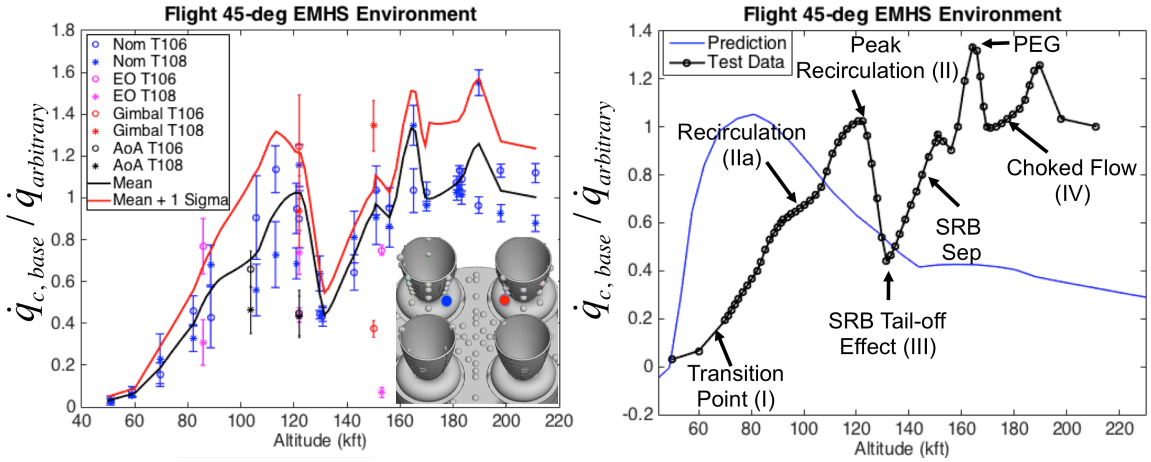

Fig 14. Normalized flight mean and mean + 1 sigma convective heat flux test data vs. altitude (left) and normalized flight mean test data and prediction heat flux vs. altitude at the 45-deg in-board EMHS region (right)

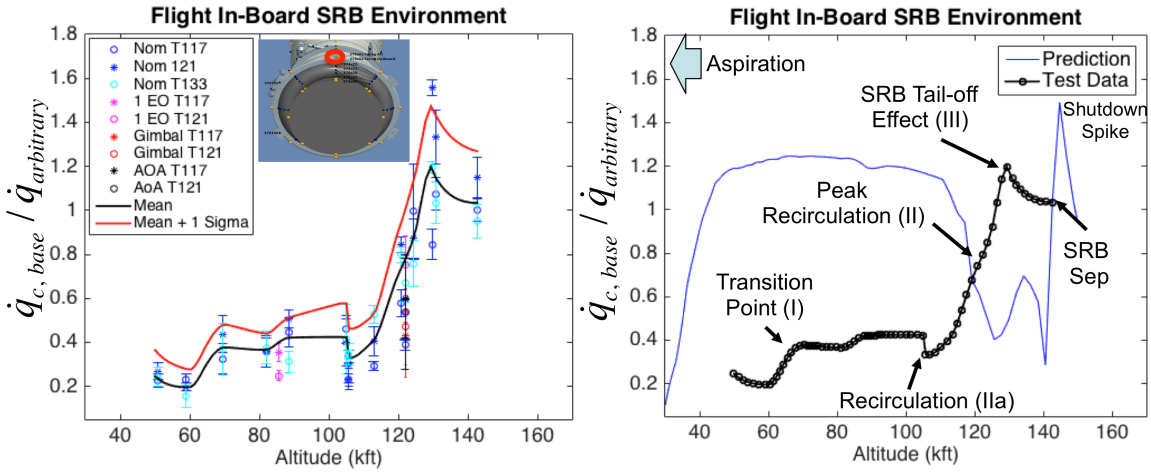

Fig 15. Normalized flight mean and mean + 1 sigma convective heat flux test data vs. altitude (left) and normalized flight mean test data and prediction heat flux vs. altitude at the in-board SRB region (right)

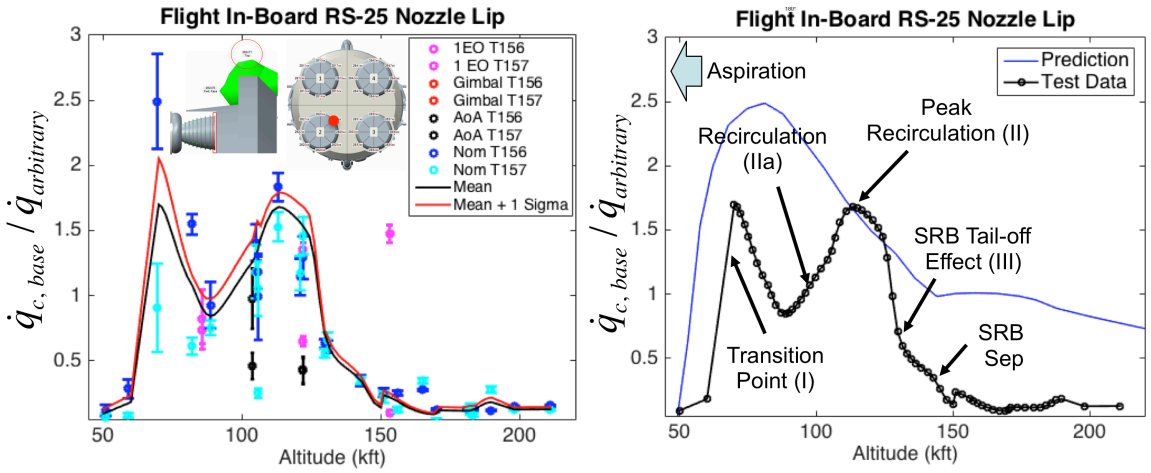

Fig 16. Normalized flight mean and mean + 1 sigma convective heat flux test data vs. altitude (left) and normalized flight mean test data and prediction heat flux vs. altitude at the 45-deg in-board RS-25 nozzle lip (right)

III. Test-Derived Flight Design Environments

A. Methodology

This section describes the methodology of deriving flight design environments from the ATA-002 raw test data and shows some results of the base flight design environments. Before design environments can be presented, a detailed description of the methodology is shown. Figure 17 shows a flow chart of the various components necessary to generate base design environments. It can be seen that once the ATA-002 raw test data (between 50 and 211 kft) is obtained, the mean and averaged convective heating data is scaled using the standard Colburn turbulent flat plate heating correlation. The scaled data adds a one-sigma uncertainty due to temporal and spatial variability. Vehicle maneuvering effects such as PEG and RS-25 program test inputs (PTI) are incorporated into the data[13]. To account for flight design environments below 50 kft, an aspiration model based on historical data is generated. Extrapolation of the design environments above 211 kft to ~500 kft is developed from ATA-002 base pressure trends. Once these models are incorporated to the scaled ATA-002 test data, the convective heating design environments from 0 kft to ~500 kft is mainly determined. NASA uses GRAD and RMC radiation code to determine multi-plume radiation acting on the base[14]. The convective heat transfer coefficient and recovery temperature vs. nozzle lip to freestream pressure ratio are inputs to the MINIVER code[14], developed by NASA. The convective heat transfer coefficient is obtained from test data and the recovery temperature is obtained from non-intrusive tunable diode laser absorption spectroscopy (TDLAS). TDLAS design, operation, reduction of data and results are presented in *Parker et al* [2016][15]. MINIVER, using Monte Carlo simulation, integrates the test data with the 2000 flight trajectories and picks out the worst-case trajectory from a heat load perspective. MINIVER incorporates BSM impingement and SRB shut-down effects on the base which are determined through computational fluid dynamics (CFD) and test data analyses developed by NASA[16]. Prior to generating finalized environments, core auxiliary power unit (CAPU) exhaust flow effects are added to the plume-induced convection and radiation heating of the base. CAPU models are developed using CFD[17]. Once all these models have been incorporated, the final design environments are verified and inspected. In summary, all the other models incorporated are based on numerical predictions except the base convective heating from 50 kft to 210 kft which uses wind-tunnel test data.

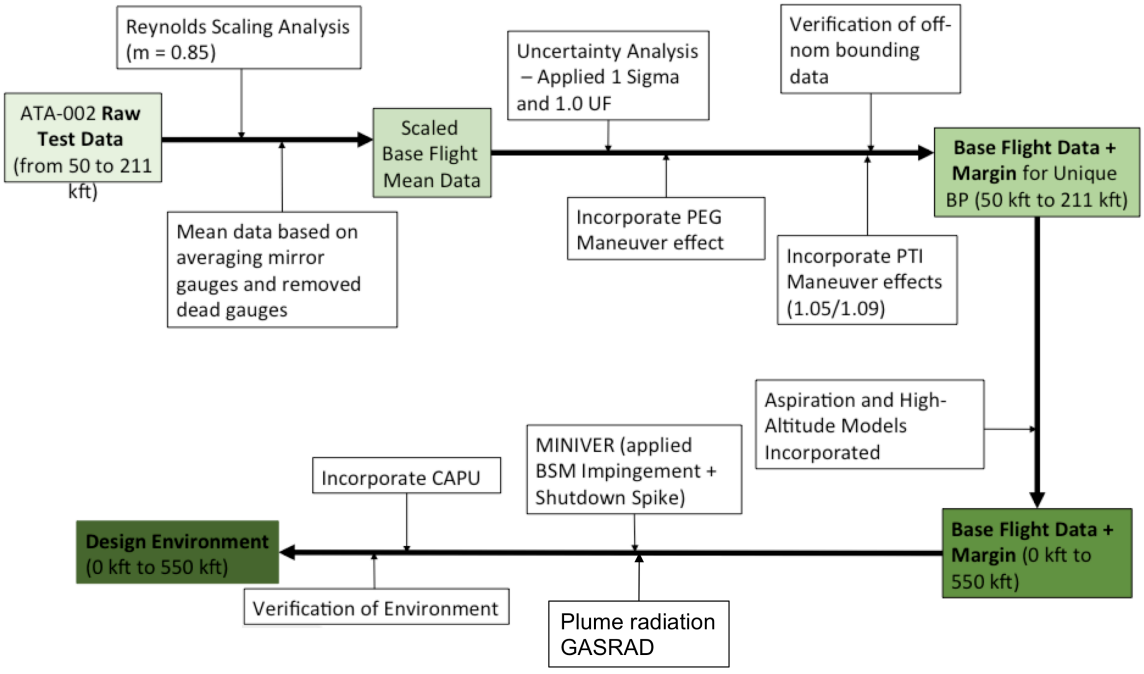

Fig 17. Flow diagram of processes to convert wind tunnel base heating test data to flight design environments

The Colburn turbulent flat plate correlation is shown in the below equations. Colburn correlation is only viable if the four assumptions are satisfied as presented below[18]. The first two assumptions are satisfied since the oxidizer to fuel (O/F) ratio between the test and flight are matched as shown in *Dufrene et al* [2016][4]. The third assumption is actively pursued in the ATA-002 tests and is adequately satisfied. It is critical to match the Plip/Pinf ratio since this matches the inviscid flow physics. The other main nondimensional numbers that are satisfied are the freestream and plume Mach numbers, Prandtl number and the normalized nozzle boundary layer specific enthalpy. The fourth assumption is relatively satisfied based on the ATA-002 Reynolds scaling test results. The flight convective heat flux is determined from last equation. The Reynolds exponents are determined through analysis of turbulent flat plate theory and Reynolds scaling ATA-002 test results.

There are two main SLS maneuvers that directly play a role on base convective heating as shown in Figure 18: (a) PEG and (b) PTI. PEG maneuver pitches the vehicle away from the boosters during SRB separation to prevent recontact and lasts for ~10 kft. This maneuver is also necessary to achieve lunar retrograde orbit. All four RS-25 engines are gimbaled in the same orientation and this configuration has been tested during ATA-002. There is no roll component to this maneuver. The PTI maneuvers are not coordinated RS-25 gimbal maneuvers and present a more random component, which are not explicitly tested during ATA-002.

$$Nu_b = C\,\mathrm{Re}_b^m \mathrm{Pr}_b^n$$

Assuming: (1) $\mathrm{Pr}_{test} = \mathrm{Pr}_{flight}$ (O/F ratio matched)

(2) $T_{g-test} = T_{g-flight}$ (O/F ratio matched)

(3) $\left(\frac{P_{lip}}{P_\infty}\right)_{test} \approx \left(\frac{P_{lip}}{P_\infty}\right)_{flight}$

(4) $P_{base} = k_2 P_c$ (Valid based on theory)

$$\dot{q} \propto k_1 P_b^m D^{m-1} = k_1 k_2 P_c^m D^{m-1} \quad (\text{assuming } P_b = k_2 P_c^1)$$

$$\frac{\dot{q}_{test}}{\dot{q}_{flight}} \propto \left(\frac{P_{c-test}}{P_{c-flight}}\right)^m \left(\frac{D_{test}}{D_{flight}}\right)^{m-1}$$

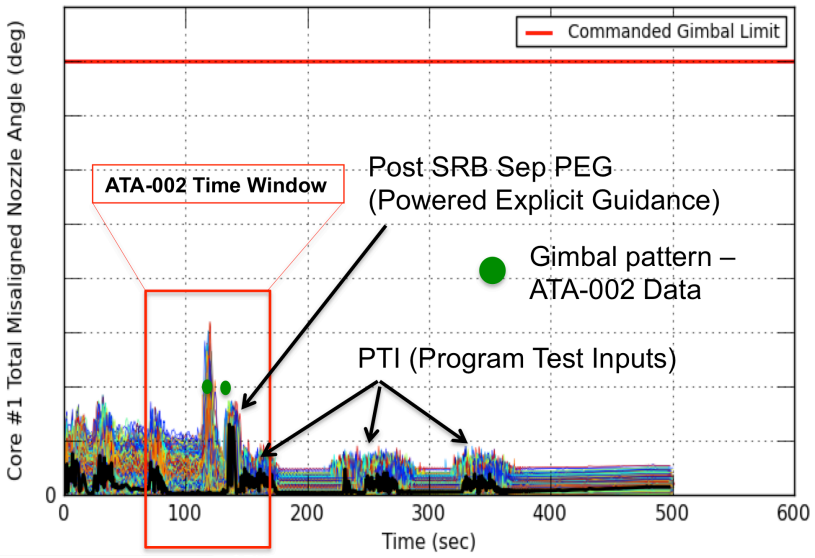

Fig 18. Core #1 total misaligned nozzle angle vs. time

B. SLS External Base Thermal Design Environments

Figures 19-22 show the normalized base design thermal environments between pre and post-test. Pre-test heating distributions are derived from semi-empirical numerical models. NASA and Boeing used the pre-test base design environments for vehicle design prior to SLS critical design review (CDR). Post-test distributions are obtained from the ATA-002 test data and it is the finalized base design environments that NASA and Boeing are now working toward post-CDR. Figures on the left and right are normalized convective and total heating rate – altitude distributions, respectively. The total heating rates is the addition of plume-induced convection and radiation components. In these figures, the SLS vehicle maneuvers, shutdown spike, BSM impingement, CAPU effects and SRB separation are marked.

The shutdown spike is an event that occurs during booster tail-off when the thrust is less than 10% of maximum thrust prior to booster separation. Burning the end of the solid propellant leads to development of aluminum-oxide slag within the combustor. This led to expulsion of the slag through the nozzles, which results in high base radiation and convection heating as shown in Figures 19-22. The shutdown spike model developed by NASA from Shuttle and previous launch vehicle test data was used to predict the SLS event's environment. BSM impingement is when the BSM plumes are fired to separate the boosters from the core-stage. This ~0.5 second firing leads to BSM plume impingement on the RS-25 nozzles and engine fairing as the boosters are separating. The base convective and radiation heat flux environments due to BSM impingement are predicted from CFD and GRAD solutions, respectively. Two CAPU exhaust ports are positioned towards the periphery (N-S) of the BHS in the vent regions. These ports are used to vent hydrogen, the fluid used for the RS-25 gimbal actuators. There is concern that the very low CAPU exhaust mass flow rate would mix with the oxygen-air and ignite due to hot recirculating base flow. *Morris* [2015] developed a CAPU convective base heating prediction model, based on CAPU operating conditions and various CFD solutions[19]. CAPU effects were significantly diminished after 100 kft due to the lack of freestream oxygen. However, CAPU showed high convective heating rates for altitudes below 50 kft, where maximum rates were observed locally around the CAPU ports[19]. A blue shaded region in Figure 19 shows the altitude range of ATA-002 testing.

The test-derived base thermal design environments showed that two regions have much higher convective and total heating rates than pre-test environments: (a) BHS (Figure 19) and (b) EMHS (Figure 20). The post-test peak convective heating at 121 kft is higher than pre-test by a factor of ~1.5 for these two regions. It can be seen that the post-test core-only flight total heating design environments are twice and four times as high as prediction for the BHS center and in-board EMHS regions, respectively. Since the core-only flight accounts for ~75% of the flight duration, this significantly increases the total heat load within these components as shown in Table 1. Although not presented in this paper, all locations on the BHS show higher core-only flight heating by a factor of 2 to 4 times than pre-test environments. All four in-board EMHS regions from 0-deg to 90-deg for post-test environments show much higher heating by similar factors than pre-test (not shown in this report). There is higher post-test heating observed at RS-25 nozzle hat-band 3 than pre-test environments as shown in Table 1 which is due to the high heating observed on the EMHS. Plume-induced convection is dominant above 50 kft and radiation is dominant below this altitude for most of the locations on the base. The base center heat load percentage contribution due to convection is ~85% for post-test, which is higher than that observed for Shuttle and Saturn vehicles.

The SRB base and RS-25 nozzle lip have more benign post-test design environments than pre-test as shown in Figures 21 and 22. The booster-in board base design environments show high heating at 131 kft due to the SRB tail-off effect, but peak convective and total heating is dominated by the SRB shutdown spike as shown in Figure 21. The pre-test environments do not adequately capture the onset and a much larger duration of peak heating is predicted. CAPU has a minimal effect on the SRB base and heat loads are comparable between post and pre-test environments. RS-25 nozzle lip heating is substantially reduced during core-only flight due to large nozzle spacing and the absence of the high momentum RSRMV plumes (Figure 22). High nozzle lip heating is observed early in flight due to RSRMV plume interactions with the RS-25 nozzle.

Table 1 shows normalized total heat loads of pre-test and post-test design environments. These base plume-induced heat loads of various base components are normalized by the total heat load at an arbitrary location on the vehicle to show scale. There are large increases between post and pre-test environments for the BHS, EMHS and certain regions of the RS-25 nozzle. However, the heat load in this region is about ~10 times the load for an arbitrary region. Base heating has the highest heat loads on the vehicle. Peak heating rates and total heat load both govern the design of the type and amount of thickness needed for the

thermal protection system (TPS). Peak heating rates determines the type of TPS and the total heat load determines the TPS thickness.

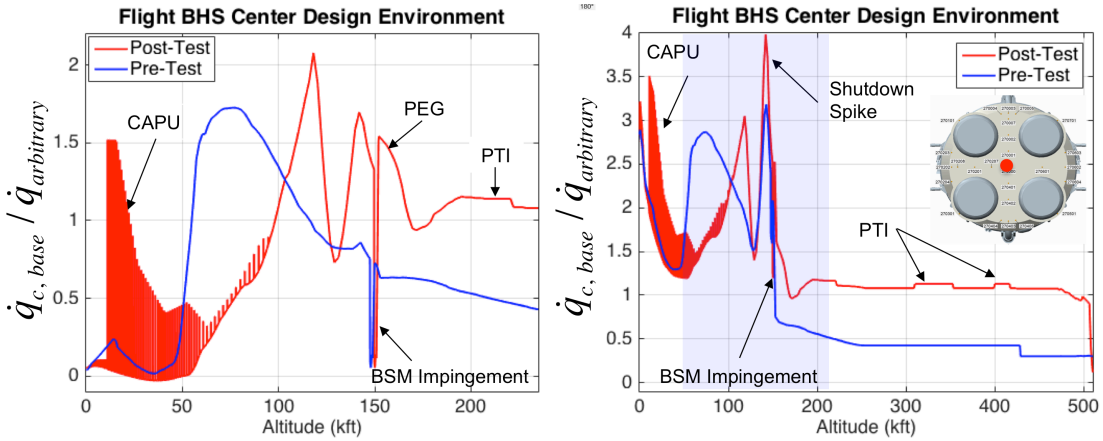

Fig 19. Normalized flight convective (left) and total (right) heat flux design environments vs. altitude at the BHS center

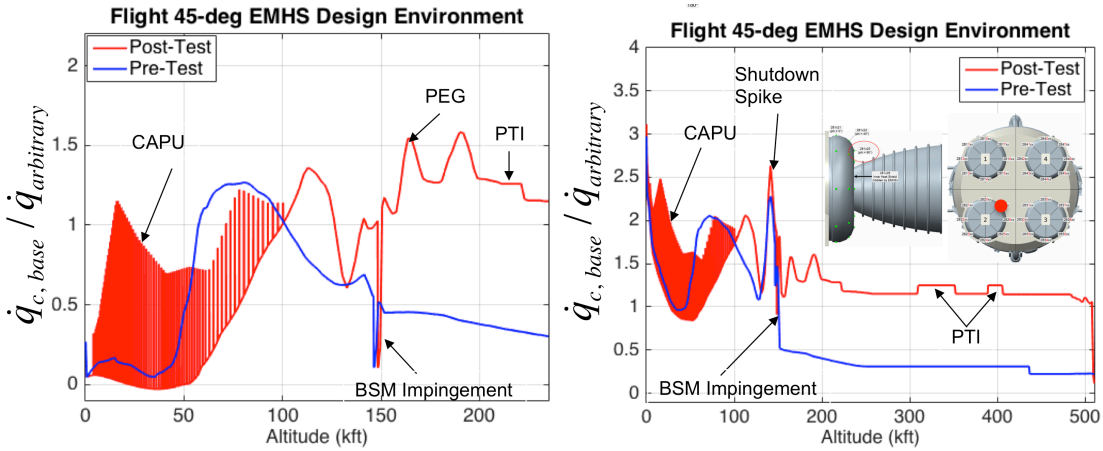

Fig 20. Normalized flight convective (left) and total (right) heat flux design environments vs. altitude at the 45-deg in-board EMHS region

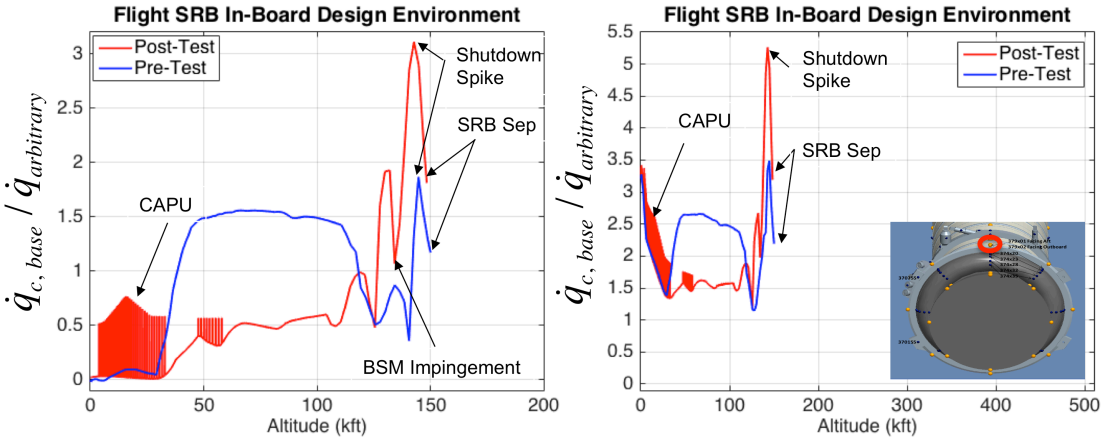

Fig 21. Normalized flight convective (left) and total (right) heat flux design environments vs. altitude at the in-board SRB base region

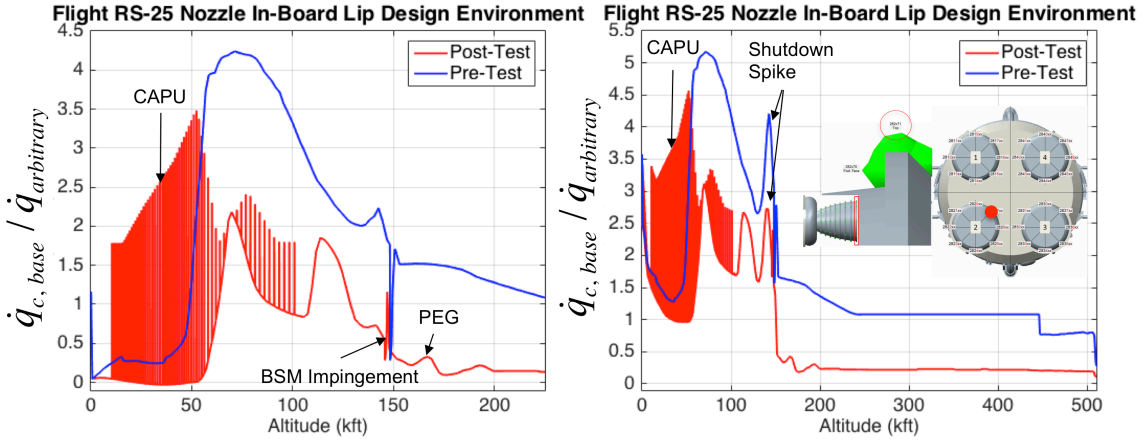

Fig 22. Normalized flight convective (left) and total (right) heat flux design environments vs. altitude at the 45-deg in-board RS-25 nozzle lip

Table 1. Normalized Heat Loads for SLS Base Components

Base Regions	Normalized Values		
	Post-Test Heat Load	Pre-Test Heat Load	Post/Pre Heat Load Ratio
BHS Center	9.9	6.6	1.5
EMHS 45-deg In-Board (phi = 45 deg)	9.4	5.0	1.9
EMHS 45-deg In-Board (phi = 0 deg)	8.2	2.4	3.5
SRB In-Board Base	4.1	4.7	0.9
RS-25 In-Board Nozzle Lip	4.9	11.2	0.4
RS-25 In-Board Nozzle Hat-Band 3	10.0	5.1	2.0

IV. Base Thermal Impact

The final objective of the ATA-002 wind tunnel program was to determine the thermal impact to the base of the SLS vehicle. This could only be assessed if high-fidelity base thermal environments were obtained which was the goal of ATA-002. Based on the presentation of post-test design environments in Section 3, it is quickly concluded that the main areas of concern for the base are the EMHS and BHS.

The EMHS protects the RS-25 turbomachinery and gimbal actuators from overheating and if the temperature in this region exceeds design limits, this could compromise the turbomachinery seals and other components. The EMHS is composed of attach brackets to the BHS and structural support battens as shown in Figure 23. Thermal blanket conforms to these battens and protects the internal cavity from high heating and breach. The BHS is a critical component as it protects the avionics, RS-25 engine controller unit, the electrical boxes and cables for the engines and the RS-25 engine power head. The base heat shield has a layer of TPS to keep BHS substrate temperatures below the design limit.

The post-test EMHS design environments are challenging the current thermal blanket designs due to significantly higher heat loads it will experience during flight than pre-test. The internal compartments around the RS-25 engines currently exceed their temperature limit and as a result Boeing and NASA are in the process of redesigning and assessing the EMHS thermal blanket. Based on the post-test design environments, the TPS on the BHS will ablate and erode as a function of time, but the goal is to make sure that the substrate metal temperature is within design limits during the full-duration of flight. Figure 23 shows how much of the TPS is left after the full-burn of the propulsion system. As can be seen the base center sees much deeper and larger area of TPS erosion for the post-test environments than pre-test as

would be expected. The TPS near the CAPU ports sees substantial erosion for both post and pre-test environments. Boeing has currently done all thermal analysis and material thermal response[20]. Boeing and NASA are in the process of improving the BHS TPS design.

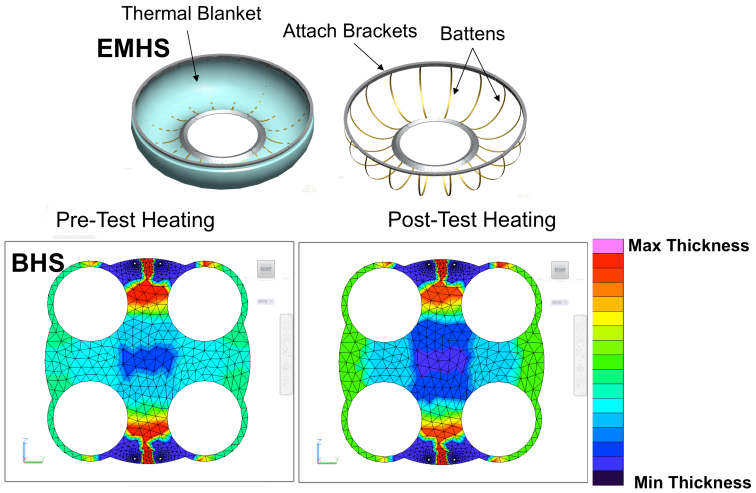

Fig 23. EMHS components (top) and BHS thickness available after SLS flight to MECO

V. Conclusions

The ATA-002 test-derived environments have provided extensive insight into the SLS base flow physics and generated higher fidelity thermal base design environments. The SLS base flow physics is highly influenced by: (a) the RSRMV plume dynamics with the freestream and its interactions with RS-25 plumes, (b) RS-25 plume dynamics with the freestream and (c) RS-25 nozzle spacing. The thermophysics are also driven by number of engines, flight trajectory, etc. High fidelity base design environments are developed from ATA-002 test data in conjunction with semi-empirical and computational models to account for SLS in-flight maneuvers, CAPU effects, plume radiation and other SRB separation related events. The design environments that deviate significantly from prediction or pre-test environments are BHS, EMHS and RS-25 nozzle base near the EMHS. This makes up the majority of the base of the vehicle. Thermal impact to these critical base components is briefly discussed. As a result, the semi-empirical models need to be updated to include the effects of the boosters and new geometry configurations. More importantly, current numerical prediction models are not able to adequately capture the complex physics and test validation is needed. As a result, hot-fire wind tunnel tests are required to obtain high-fidelity base thermal environments for launch vehicles and spacecraft to efficiently protect the vehicle.

Acknowledgement

Thanks to the testing efforts of the CUBRC engineers and technicians (Chris Halt, William Winter, Dan Czora, Daniel Sargent, Salvatore Russo, Gary Paone, Rick Steele, Robert Field, Vince Smith, Joseph Ziemba, Dr. Matt MacLean, Dr. Ron Parker and Dr. Zakery Carr) and the technical advice, test support and analyses of NASA MSFC (Dr. Chris Morris, Mark D'Agostino, Darrell Gaddy, Adam Kimberlin, Brandon Mobley, Craig Schmitz and Dr. Francisco Canabal) and NASA Johnson Space Center (Jeff Vizcaino, Molly White and Katie Boyles).

References

[1] Mehta, M. et al (2014), Space Launch System (SLS) Pathfinder Test Program: Sub-Scale core-stage (CS) rocket engine development for short-duration testing, Aerosciences Branch/EV33 (14-021) Technical Memorandum, NASA Marshall Space Flight Center, Huntsville, AL.

[2] Mehta, M. et al (2014), Space Launch System (SLS) Pathfinder Test Program: Sub-Scale booster solid rocket motor development for short-duration testing, Aerosciences Branch/EV33 (14-023) Technical Memorandum, NASA Marshall Space Flight Center, Huntsville, AL.

[3] Dufrene, A. et al (2016), Space Launch System (SLS) Base Heating Test: experimental operations and results, AIAA Paper: 231-5920, 54th AIAA Aerospace Sciences Meeting, AIAA Science and Technology Forum and Exposition 2016, San Diego, CA.

[4] Parker, R. et al (2016), Space Launch System (SLS) Base Heating Test: tunable diode laser absorption spectroscopy, AIAA Paper: 231-5920, 54th AIAA Aerospace Sciences Meeting, AIAA Science and Technology Forum and Exposition 2016, San Diego, CA.

[5] Morris C. I. (2015), Space Launch System (SLS) ascent aerothermal environments methodology, AIAA Paper: 231-5920, 53rd AIAA Aerospace Sciences Meeting, AIAA Science and Technology Forum and Exposition 2015, Kissimmee, FL.

[6] Hirschel, E.H. (2015), Basics of Aerothermodynamics, Springer: New York, NY.

[7] Mehta, M. et al (2015), DAC3R Rev A Environments, Aerosciences Branch, NASA Marshall Space Flight Center, Huntsville, AL.

[8] Kim, J.G. et al (2011) Investigation on the characteristics of plume induced flow separation and wall heat transfer, AIAA Paper: 2011-711, 49th AIAA Aerospace Sciences Meeting, Orlando, FL.

[9] Engel, C.D. and S.C. Praharaj (1983) MINIVER upgrade for the AVID system. Volume 1: LANMIN user's manual, NASA-CR-172212, RemTech Inc., NASA Marshall Space Flight Center, Huntsville, AL.

[10] Bender, R.L. (1981), JANNAF Handbook Rocket Exhaust Plume Technology: Chapter 5 Base Flow, Chemical Propulsion Information Agency, Johns Hopkins University, Applied Physics Laboratory, Laurel, MD.

[11] Mehta, M. et al (2014), Numerical base heating sensitivity study for a four-rocket engine core configuration, *AIAA JSR*, Vol. 50, No. 3, pp. 508 – 526.

[12] Morris, C.I. (2016), CAPU heating, Aerosciences Branch/EV33 Technical Presentation, NASA Marshall Space Flight Center, Huntsville, AL.

[13] NASA Marshall Space Flight Center, RMC Code, NASA Technology Transfer, 2015.

[14] Emery, B. (2015), Core Stage VAC2C Heating Environments - Assessment 2 of NASA Level 2 DAC3R w/ATA-002 & Boeing Refined CAPU Heating Environments, Boeing Core-Stage Thermal Analysis, Technical Presentation, NASA Marshall Space Flight Center, Huntsville, AL.

[15] Musial, N.T. and Ward, J.J. (1961) Base flow characteristics for several four-clustered rocket configurations at Mach numbers from 2.0 to 3.5, NASA Technical Note, TND-1093, NASA Marshall Space Flight Center, 1961.

[16] Brewer, E.B. and C.E. Craven (1969), Experimental investigation of base flow at high-altitude for a four-engine clustered nozzle configuration, NASA Technical Note, NASA TND – 5164, NASA Marshall Space Flight Center.

[17] Goethert, B. H. "Base Flow Characteristics of Missiles with Cluster-Rocket Exhausts," Institute of Aeronautical Sciences (IAS) Paper 60-89. 1960.

[18] Mullen, C. R., Bender, R. L., Bevill, R. L., Reardon, J., and Hartley, L. (1972), Saturn Base Heating Handbook, The Boeing Company, NASA CR-61390, Huntsville, AL, 1972.

[19] Sergeant, R. J. (1965), Base Heating Scaling Criteria for a Four-Engine Rocket Cluster Operating at High Altitude, AIAA Aerothermochemistry of Turbulent Flows Conference. San Diego, CA, AIAA 65-826, 1965.